NASA Technical Memorandum 107146

Steady Capillary Driven Flow

Mark M. Weislogel
Lewis Research Center
Cleveland, Ohio

February 1996

National Aeronautics and
Space Administration

Steady Capillary Driven Flow

Mark M. Weislogel
NASA Lewis Research Center

ABSTRACT

A steady capillary driven flow is developed for a liquid index in a circular tube which is partially coated with a surface modifier to produce a discontinuous wetting condition from one side of the tube to the other. The bulk flow is novel in that it is truly steady, and controlled solely by the physics associated with dynamic wetting. The influence of gravity on the flow is minimized through the use of small diameter tubes $\sim O(1mm)$ tested horizontally in a laboratory and larger tubes $\sim O(10mm)$ tested in the low gravity environment of a drop tower. Average steady velocities are predicted and compared against a large experimental data set which includes the effects of tube dimensions and fluid properties. The sensitivity of the velocity to surface cleanliness is dramatic and the advantages of experimentation in a microgravity environment are discussed.

I. Introduction

The capillary driven flows to be discussed are constrained to capillary flows where spatial gradients in the interfacial tension, σ, are absent ($\nabla \cdot \sigma = 0$). Such flows exist solely as a result of system geometry and surface wettability and though they are ubiquitous in nature and industry they are particularly conspicuous in low gravity environments such as those produced aboard orbiting space craft. In this study, a simple experimental technique is adopted which permits the observation of purely capillary driven flows which are steady. Such flows may prove useful as a tool to study fundamental characteristics of capillary flows relevant to many fluids management processes. The reported experiments are intended to be 'demonstrative' of this possibility.

In fig. 1 a right circular cylindrical tube partially filled with a liquid index is sketched in a zero gravity environment. The ends of the tube are open to the atmosphere and the left hand side of the tube is treated such that a less wetting condition (higher contact angle, θ) exists there with respect to the right hand side ($\theta_1 < \theta_2$). Since the pressure jump across a given interface is proportional to the curvature of that interface, a pressure gradient in the direction of the more favorably wetted side of the tube is established which, barring the effects of contact angle hysteresis, produces a flow resisted by the fluid's viscosity. After a brief transient, the macroscopic flow is

steady and persists as long as the liquid slug bridges the wetting discontinuity.

The earliest reference found explicitly envisioning such a flow (though there are likely to be earlier works) is that of Reynolds and Satterlee [1] who briefly discuss the case of capillary flow in tubes where the quantity $\sigma \cos\theta / r$ is not equal at both interfaces, r being the local tube radius. One special case is that of Fig. 1b which happens to produce a flow which is steady. This feature is unique in two respects: (1) It can avoid the need for transient analysis common, for instance, in similar "capillary rise" experiments [2] and (2) It is still a true capillary driven flow in which the steady fluid velocity is not maintained by, say, pump pressure, gravity head, a plunging tape, etc., but rather by the dynamic interface curvature alone.

To demonstrate the technique, a 1-dimensional analysis is performed to determine the steady average velocity, V, of a liquid index of length l, viscosity μ, density ρ, and surface tension σ, in a tube of radius r, with air as the host medium. Simple experiments are then outlined and data presented for tests performed using small capillary tubes ($r \leq 1.0mm$) in a laboratory and larger capillary tubes ($r \leq 5.0mm$) in a drop tower. The experimental results are scaled and presented against the independent variables of the problem. A brief discussion follows. It is no surprise that these flows are quite sensitive to the level of cleanliness of the tubes and that reproducibility and predictability are greatly increased with increased control of the surface conditions. Such sensitivity to surface conditions may make these flows ideally suited for studies of capillary flows over heterogeneous surfaces where the "heterogeneous" nature of the surface is highly controlled. For examples of such studies see [3-4].

II. 1-D Analysis; Average Steady Velocity

A sketch of the slightly generalized problem of interest is provided as fig. 2. The principal assumption, evident in the figure, is that the menisci can be approximated as spherical caps. This requires that the Weber, Bond, and Capillary numbers are small, $We = \rho r V^2/\sigma \ll 1$, $Bo_r = \rho g r^2/\sigma \ll 1$, and $Ca = V\mu/\sigma \ll 1$, where g is the acceleration field strength. A 1-dimensional analysis follows naturally incorporating the further assumptions of a quasi steady Poiseuille velocity profile, $\nu t/r^2 \gg 1$, where $\nu = \mu/\rho$ and t is time, a slug length such that $r/l \ll 1$ (reducing the need to account for 2-dimensional effects in the vicinity of the menisci), constant properties, slug length, tube radius, and the use of a dynamic contact angle simplification. With this, the resulting force balance is written directly

$$m\frac{dV}{dt} = F_\sigma - F_\mu + F_g \tag{1}$$

where the forces due to surface tension, viscosity, and gravity are $F_\sigma = 2\pi r\sigma(\cos\theta_1 - \cos\theta_2)$, $F_\mu = 8\pi\mu l V + 8\pi\mu_g(L-l)V$, and $F_g = \pi\rho r^2 l g \sin\phi$, respectively. m is the

mass of the slug, θ_1 and θ_2 are the "apparent" dynamic advancing and receding contact angles,[1] and ϕ is the tube tilt angle with respect to the tube axis. μ_g is the gas viscosity and L is the overall tube length. The horizontal is defined by the orientation of g, and ϕ is chosen positive in the counter clockwise direction. In the limit of low Capillary number the apparent dynamic contact angle is often defined in the literature as the geometric angle determined by extrapolating the bulk meniscus curvature to the wall. Angles defined as such are functions of Ca and are often determined by empirical techniques such as that used by Hoffman [5]. The quantity $\cos\theta_1 - \cos\theta_2 \equiv \Delta\cos\theta$ is thus a function of V and the steady value of V can be solved iteratively with empirical data for θ_1 and θ_2 as functions of Ca. A less empirically burdensome result for V may be obtained by assuming $\Delta\cos\theta \approx const.$ This choice does not alter the value of V at long times and allows the integration of eq. (1) which gives

$$V = \frac{\sigma}{4\mu}\frac{r}{l}M^{-1}\left(\Delta\cos\theta + \frac{Bo_r}{2}\frac{l}{r}\sin\phi\right) \tag{2}$$

for the steady average velocity with

$$M = 1 + \frac{\mu_g}{\mu}\left(\frac{L-l}{l}\right)$$

Entrance/exit region effects in the gas phase have been ignored. The body force and transient terms may be ignored by proper selection of fluid properties, tube Bond number, and tilt angle such that

$$\frac{Bo_r}{2}\frac{l}{r}\frac{\sin\phi}{\Delta\cos\theta} \ll 1 \tag{3}$$

With these further simplifications, eq. (2) reduces to

$$V = \frac{\sigma}{4\mu}\frac{r}{l}M^{-1}\Delta\cos\theta \tag{4}$$

which is the solution to Washburn's equation [6] where the driving pressure gradient is given by $\Delta P = 2\sigma\Delta\cos\theta/r$.

A similar analysis applied to a U-shaped circular tube, pictured in fig. 3, can also be performed for a 'U-tube' of U-bend diameter D_u (the subscript u refering to the U-tube configuration, refer to figure for notation). Assuming the menisci reside at $z = 0$ at $t = 0$, the body force term of eq. (1) is modified, $F_g = \pi\rho r^2 g\,(D_u\cos\phi + 2h\sin\phi)$, and when back-substituted into (1) and integrated over time produces

$$V_u = \frac{\sigma}{4\mu}\frac{r}{l}M^{-1}\left(\Delta\cos\theta + \frac{Bo_r}{2}\frac{D_u}{r}\cos\phi\right)\left(1 - \frac{gr^4}{16\nu^2M^2l}\sin\phi + \frac{\sigma t}{4\mu l}\frac{Bo_r}{M}\sin\phi\right) \tag{5}$$

[1]Use of the dynamic contact angle simplification is made with reluctance and though it captures much of the physics manifest at the contact line its use signals the 'demonstrative' nature of this work.

for the velocity of the liquid slug. The effects of tube curvature on the presumed Poiseuille flow profile are not considered. $h = h(t)$ is the location of the advancing meniscus as measured from $z = 0$ and the result of eq. (5) is appropriate in the limits

$$\frac{gr^4}{8\nu^2 M^2 l}\sin\phi \ll 1, \qquad \frac{gr^2 t}{4\nu M l}\sin\phi \ll 1, \qquad \text{and} \qquad \frac{8M\nu t}{r^2} \gg 1 \tag{6}$$

The behavior of V_u is not steady, as was the case for the straight tube, unless $Bo_r \equiv 0$, or $\phi \equiv 0$,[2] at which point V_u reduces to V of eq. (4).

For large r it is clear that the third constraint of eq. (6) will be difficult to satisfy for small t. When this is the case, inertia plays a significant role in the initial transient behavior of the flow as well. The two time scales are identified below and characterize the transients associated with viscous diffusion and inertia, respectively:

$$t_{visc} \sim \frac{r^2}{8M\nu} \qquad \zeta^2 \gg 1 \tag{7}$$

$$t_{inert} \sim \left(\frac{\rho l r^2}{2\sigma\Delta\cos\theta}\right)^{1/2} \qquad \zeta^2 \ll 1 \tag{8}$$

An effective damping ratio can be defined by

$$\zeta = \left(\frac{32\nu^2\rho l M^2}{r^2\sigma\Delta\cos\theta}\right)^{1/2} \tag{9}$$

The time scales of eq.s (7) and (8) are not mutually exclusive since, provided l and L are of sufficient size, $t \sim r^2/8M\nu$ will eventually dominate regardless of the value of ζ. Therefore, the system transient for the case $\zeta^2 \ll 1$ will consist of the combined effects of short term inertia giving way to longer term viscous diffusion. When $\zeta^2 \gg 1$, inertia plays no role and the system transient is $t \sim r^2/8M\nu$. These scales can be used effectively to size potential test configurations.

The complete form for $h(t)$ for the U-tube configuration is determined by noting $V_u = dh/dt$ and by integrating eq. (1) with $h(0) = V_u(0) = 0$ to give the dimensionless result

$$h^*(t^*) = \frac{Ja_1}{(a_1 - a_2)\sin\phi}\left(\exp[a_2 t^*] - 1 - \frac{a_2}{a_1}(\exp[a_1 t^*] - 1)\right) \tag{10}$$

where

$$J = \frac{r}{Bo_r l}\left(\Delta\cos\theta + \frac{Bo_r}{2}\frac{D_u}{r}\cos\phi\right)$$

$$a_1,\ a_2 = -4 \pm 4\left(1 + \frac{k\sin\phi}{8}\right)^{1/2}$$

[2]This analysis does not (but could) treat the flow when the trailing meniscus enters the 'bend' in the U-portion of the tube.

and

$$k = \frac{gr^4}{\nu^2 M^2 l}$$

with $h^* = h/l$ and $t^* = \nu M t/r^2$. Fig. 4 shows a plot of $h^*(t^*)$ and $V_u^*(t^*)$ determined from eq. (10) and its derivative, respectively, for the the case of a $1cS$ silicone oil index with $l = 131mm$, $r = 5mm$, and $\phi = -\pi/2$ (The test data for this case will be presented in fig. 10). Several gravity levels are given which are assumed constant. The qualitative nature of the solution reveals a first accelerating and then decelerating behavior of the bulk flow which for this parametric range is quite sensitive to gravity level.

From equations (2) and (5), the capillary flow velocity resulting from a discrete change in surface wettability is to a large degree proportional to r/l and, thus, the flow rate $\dot{Q}$ is proportional to r^3/l. If the constraining conditions on eq. (2) or (5) are satisfied, the r^3 dependence of the flow rate implies that substantial increases in $\dot{Q}$ can be realized in low-g environments where $r \sim O(1cm)$ as opposed to the terrestrial environment where $r \sim O(1mm)$.

III. Experimental

Two tube configurations were selected for experimentation purposes to maximize the range of tube internal diameters which could be tested. Straight capillary tubes were used to observe the smaller tube diameter range whereas the U-tube configuration was used to observe the larger diameters. The U-tube tests were performed in the 2.2 second drop tower at NASA's Lewis Research Center. The relevant tube dimensions are given in table 1. The specific experimental procedures for each test will be described shortly.

For every test a portion of the tube interior was coated with the surface modifier FC-723 to yield the variation in surface wettability necessary to drive the flow. This was accomplished by partially dip-coating the tubes in a bath of FC-723 and allowing ample time to dry. As specified by the manufacturer of the coating (3M Corporation), a flourochemical polymer surface coat approximately $0.25\mu m$ in thickness could be readily applied to the interior of a desired portion of the tubes. The coating dried rapidly and showed no measurable traces of aging beyond several hours of room temperature cure. In this manner an essentially discontinuous wetting condition was achieved at the coating boundary.[3] The uncoated portions of the tubes were completely wetted by the silicone oils, static contact angle $\theta_1 = 0$.

[3]A more gradual variation in surface wettability could be produced by promoting evaporation at the coating boundary during the coating process. In fact, an essentially continuous change in contact angle can be established with a similar yet more controlled process. For an interesting illustration of this technique see [7].

The static advancing and receding contact angles for the test fluids were determined in straight capillary tubes coated entirely with FC-723. These results along with the relevant fluid properties of the silicone oil test fluids are provided in table 2. The advancing values are included to provide the hysteresis band for the fluid/solid pairs. The static hysteresis band could be determined by solving equation (2) for $\Delta \cos\theta$ with $V = 0$ yielding

$$\frac{Bo_r}{2}\frac{l}{r}\sin\phi = \Delta\cos\theta$$

which gives the maximum liquid mass which contact angle hysteresis will support. ϕ was increased to the point at which flow was "almost" induced. At this point θ_{adv} and θ_{rec} were inferred via the geometric relationship

$$\theta = \sin^{-1}\left(\frac{1-\alpha^2}{1+\alpha^2}\right)$$

with $\alpha = z_i/r$, z_i being the meniscus height at the advancing ($i = 1$) and receding ($i = 2$) menisci (refer fig. 2). This was also the method used for the dynamic contact angle measurements, out of necessity, to accommodate for interface distortions due to mismatched tube/fluid refractive indices.

1. Straight Tube Tests. A given straight capillary tube, once cleaned and coated, was charged with a liquid slug of prescribed length introduced from the coated end of the tube. The tube was then tilted with respect to gravity until the slug began to flow towards the boundary of the coating. When this boundary was reached, the fluid rapidly achieved a steady velocity in the direction of the uncoated side of the tube. At this point the tube was immediately placed on a level glass table, the entire process being backlit and filmed with a variable speed cine camera directed vertically downward at the tube. Due to the magnification of the camera required to resolve the meniscus ($< 8mm$ FOV) and the long slug lengths tested (up to $\sim 300mm$), it was necessary to move some of the tubes during the flow from the advancing meniscus to the receding meniscus. This "move" was made as a discrete step between ample periods of cine camera photography on the advancing and receding meniscus regions. The glass table was leveled to the degree necessary to satisfy eq. (3). This required the use of a precision level and grades of less than $170\mu m/m$ ($\phi < 0.01°$) were maintained.

The uncertainties particular to the straight tube tests and unaccounted for in the development of eq. (2) are the transients required to establish a fully developed flow, entrance/exit region effects, and non-axisymmetric menisci attributable to the gravity field being perpendicular to the tube axis. For the typical test fluids, tube radii, slug lengths, and the resulting flow velocities $\sim O(1cm/s)$, these effects could be estimated separately and shown to have little effect ($< \pm 5\%$) on the steady velocities measured.

2. U-tube Tests. The U-tube approach was adopted as a simple means to maximize the $2.2s$ of low gravity time afforded by the $23m$ drop tower. The initial condition

was such that the liquid slug strattled the coating boundary prior to the release of the experiment apparatus into free fall. The step reduction in gravity marked the onset of capillary driven flow. Fig. 5 shows a selection of frames for two such tests. Backlighting and high speed cine camera photography were employed for the data collection.

In addition to the entrance/exit region and transient effects, mentioned previously for the straight tubes, three further causes for increased uncertainty were introduced by the U-tube approach. These were centrifugal effects, a tube eccentricity effect at the bend due to their fabrication, and an additional transient necessary for the normal gravity menisci to establish their low-g surface shapes. Each of these were examined independently and a cumulative error estimated to be no more than $\pm 10\%$ of V_u.

Tube Interior Surface Conditions. As has been shown by numerous investigators, the interior surface condition of the tubes plays a most important role in capillary driven flows. To illuminate such effects, a number of tube cleaning/preparation tests were conducted similar to those of Mumley et al[8]. These tests included initially dry tubes (D), tubes which were prewet by the test fluid leaving a macroscopic film on the uncoated side of the tube (PW), and tubes which were prewet and then allowed to drain dry for several days (PD)–what Mumley et al. refer to as a prewet-dried condition. Two types of dry tube tests (D) were conducted: the "as delivered," or factory cleaned condition, where the tubes where not cleaned but tested in the condition as received from the manufacturer, and the "cleaned," or lab cleaned condition, which consisted of a series of rinse/washes in a soap solution, distilled water, acetone, methanol and/or ethanol, and a distilled water flush with air dry. A final cleaning step was attempted by baking out the cleaned tubes in a vacuum oven, but such tubes could not be coated easily by the FC-723 in a discontinuous manner. This may be in part due to increased surface diffusion of the volatile coating. Sporadic, unsteady, and often nonexistent flows resulted in such cases. The U-tubes were not tested using the PW or PD preparatory procedures.

The larger inner diameter U-tubes permitted direct contact measurements of the internal surface conditions. A lab standard surface profilometer was employed for this purpose and, as a demonstration, values for the mean, rms, and peak-to-valley surface roughness were found to be 0.04, 0.048, and $0.203\mu m$, respectively, as measured parallel to the tube axis over a $0.8mm$ sampling length (all values $\pm 50\%$). Circumferential measurements could also be made. Such information is rarely available with experimental data on flow in capillary tubes.

IV. Results

The axial location of a given meniscus was first tracked in time using a motion analyzer. Fig. 6 illustrates some results for a number of factory cleaned straight tube tests performed with 1cS silicone oil and a variety of slug lengths. As seen from the figure, the base flow is indeed steady. Time $t = 0$ here represents the initiation of data collection and not the beginning of the flow.

Deviation plots between instantaneous velocities measured experimentally and those determined by a linear fit to the data show agreement to within 1.5% or better, an agreement which is at or below the resolution accuracy of the framing rate of the cine camera. Fig. 7 provides two examples. The raw data sets were acquired using an automated image analysis technique which digitized the cine film records frame by frame and tracked the menisci across the field of view. The grabbed images were low-pass filtered and a median threshold was selected to define the interface. Only data points are shown in the figure (no line). The linear fits to the data are subtracted from h measured experimentally and the differences are shown. In fig. 7a, a worst case, the long period oscillation reveals a peak uncertainty of 1.5% for the instantaneous velocity and may reflect a slightly varying film speed. In fig. 7b no trend of the deviations is visible and discrepancies are far less than $\pm 1\%$. The general form of a given deviation plot was neither reproducible, nor traceable to a given surface condition or test configuration.

Fig. 8 displays sample U-tube data acquired similarly for several test cases where $r^2/8M\nu < 0.25s$. The initial transient is readily seen and the flows can be said to be predominately steady. The fact that a "falling off" of the velocity is present for these tests indicates the significance of the body force term, $\sigma t Bo_r \sin\phi/4\mu Ml$ in eq. (5). Given that the low-g environment of the drop tower is $\sim O(10^{-4}g_o)$ due to aerodynamic drag ($g_o = 9.8m/s^2$), taking $\phi = -\pi/2$, the principal direction of the drag force, the above term is the appropriate magnitude ($\sim 0.05t$) to produce this behavior. This effect was also observed to diminish with decreasing time, decreasing tube radius, increasing fluid viscosity, and increasing slug length. These trends are in accord with eq. (5). Fig. 9 plots the instantaneous velocity against time for the data of fig. 8. The negative linear trend is obvious. The prefactor $G = r^2/\nu l$ is introduced on the figure as a measure of the intensity of the transient term in eq. (5), where $\sigma Bo_r/\mu l = Gg$. It is apparent that the slope of the linear fits to the data are related to G as anticipated by eq. (5). For fixed g one could minimize gravitational effects for the U-tube configuration by minimizing G. It should be emphasized that the straight tube configuration adopted for use in the drop tower would eliminate this falling-off effect and that tubes with L and l of sufficient length would achieve steady flows of similar calibre to the straight tube tests of this study.

Several of the larger inner diameter U-tube tests were performed where $r^2/8\nu M \sim 3s$, which implied viscous time scales larger than the drop time available. An example is provided in fig. 10 for $1cS$ silicone oil in a $9.88mm$ inner diameter tube. The initial oscillation of the interface due to the step reduction in g is more exaggerated than for the cases of fig. 8. The decay time for these oscillations ($\leq 0.25s$) is half that predicted by a recent correlation developed for a similar step reduction in g for partially fluid-filled cylindrical containers [9]. The discrepancy is due to the additional damping influence of the bulk flow. t_{inert} for this case is approaching $1s$ and $\zeta^2 = 0.112$. The basic elements of the greater unsteadiness of the flow can be gleaned from eq. (10) which reveals a first accelerating and then decelerating flow due to the presence of finite g with $\phi = -\pi/2$ (refer to qualitative result of fig. 4). However, the analysis cannot capture the quantitative transients of these flows. This should be expected since $\Delta \cos\theta = const.$ is hardly representative of the true phenomena, the constant low-g assumption for the drop tower tests is not correct, and the constraint $8M\nu t/r^2 \gg 1$ is not satisfied.

The distance-time data were reduced to give average velocities using a central difference scheme on data such as those presented in fig. 6 and 8. At least 15 values were used in each average value. An oddity of some of the experiments was that on occasion the average velocity values determined at the advancing and receding menisci for the same liquid slug were sometimes detected to differ by as much as $\pm 5\%$. This was never true for the U-tube tests and no pattern, or test condition or configuration could be established to determine when or why this would happen. In the event of such an occurrence the advancing and receding velocities were simply averaged to determine V.

Dynamic contact angle measurements were made to within $\pm 3°$ for the wide range of tests performed, and in many cases $\pm 2°$ or better was common, the difference coming from a trade-off between accurate contact angle measurement and accurate velocity measurement. Though the point becomes mute at low Ca where measurement uncertainties of V were less than $\pm 1\%$, the higher uncertainty of $\pm 3°$ for θ incurred errors up to $\pm 25\%$ in the calculation of V from eq. (4) through $\Delta \cos\theta$. Cumulative uncertainties as high as $\pm 30\%$ for V and V_u calculated from the measured quantities could be expected in these cases. Of the many cases where contact angles could be determined within $\pm 2°$, uncertainties could be banded between $\pm 25\%$.

Eq. (4) can be rearranged to give

$$\frac{V}{\Delta \cos\theta} = \frac{\sigma}{4\mu}\frac{r}{l}M^{-1} = F \tag{11}$$

which separates the dependent from the independent parameters of the problem. The former is plotted against the latter in fig. 11 on a log-log scale. This figure represents the sum total of the study for all of the tests conducted. Eq. (11) is displayed with

an error band allowing for the estimated 25% uncertainty. Fig. 12 gives a breakout of the different tube surface conditions. As can be viewed in fig. 12a, and as will be seen shortly, not much control was afforded by the added effort of further cleaning the tubes from the state in which they were received. The cleaning for the U-tube tests (fig. 12b) was unspecified and consisted of an unknown combination of factory and lab clean conditions. The pre-existing films in the prewet tests (fig. 12c) for the straight tubes were not closely controlled or measured. By comparison, the case of the prewet and dried tubes (fig 12d) was highly repeatable and the data generally fell within the error band of eq. (11).

The standard deviation for the repeatability of the measured quantity $V/\Delta\cos\theta$ for the straight tube tests was $\pm 41\%$ for the factory cleaned tubes, $\pm 38\%$ for the lab cleaned tubes, and $\pm 4\%$ for the PD tubes with F held approximately constant. Fig. 13 presents straight tube data indicating the tube cleaning technique for each data point. As seen from the figure, the cleaning technique clearly influences primarily the degree of scatter of the data through $\Delta\cos\theta$, the PD condition exhibiting the most control. Too little U-tube test data was collected to permit reasonable statistical analysis.

Rearranging eq. (11) further gives

$$Ca = \frac{r}{4l} M^{-1} \Delta \cos\theta = F_2 \tag{12}$$

which is presented in fig. 14 using the data of fig. 11. Worthy of mention is that for purely capillary driven flows as defined herein, inspection of eq. (12) shows that the Capillary number scaled on the correct velocity, V, is a function of the geometry of the system (r/l) and the dynamic surface wettability $(\Delta\cos\theta)$. It should also be pointed out that the agreement of the data with eq. (11) is increased with the inclusion of M which accounts for the viscosity of the gas phase. No effort was made to vary M specifically and values between 1 and 1.91 were achieved.

Though the flow is relatively well represented by eq. (11), only modest correlation between θ_{adv} and Ca was established. Fig. 15 is provided as an illustrative example for the factory cleaned straight tube tests. Symbols are provided indicating tube inner diameter (fig. 15a) and fluid viscosity (fig. 15b). The correlation given by Hoffman [5] for $Ca < 0.1$ for the advancing meniscus

$$\theta_{adv} = 4.54 Ca^{0.353} \quad (radians) \tag{13}$$

is provided for reference. Without this curve sketched on the figures the global trend for θ_{adv} identified by Hoffman might not be distinguished. This is in part due to the limited range of Capillary numbers accessible by purely capillary driven flows. The data for the PD tests show little improvement. The receding contact angle values as functions of Ca are included as fig. 15c for completeness.

Fig. 16 provides the results for $\Delta\cos\theta$ with Ca for the data of fig. 15 which shows that, in this study, the larger values of $\Delta\cos\theta$ were achieved for the smaller tube radii and higher viscosity fluids.

V. Discussion

The scatter of the data displayed in fig. 11, and more specifically in fig. 13, shows the effects of surface conditions on the value of the steady capillary velocity of liquids in tubes with wetting discontinuities. It must be born in mind that in most cases each average velocity measurement was made to a relatively high degree of precision, often within 1% or better. Thus, as stated, the principal uncertainty is mainly attributed to the contact angle measurement uncertainty of $\pm 2°$ leading to an uncertainty in $\Delta\cos\theta$ of up to $\pm 25\%$. Albeit a large uncertainty, the experimentally determined spread of $V/\Delta\cos\theta$ for F fixed is even larger, up to $\pm 41\%$, for the cases of the factory and laboratory cleaned tubes. Nonetheless, the spread is still somewhat centered about eq. (11) implying that the physical effects of surface conditions of microscopic scale at the contact line are largely accommodated by changes in interface curvature observed on a macroscopic scale.

Fig. 17 displays the dynamic contact angle data as a function of Ca for the data of fig. 13. The factory and lab cleaned tubes yielded slower flows (up to three times slower than the PW tests) and hence lower values for $\Delta\cos\theta$ with increased uncertainty. The fact that the dynamic receding contact angle actually increases with increasing Ca, as shown in fig. 17, is perhaps misleading, contrary to intuition, and deserves attention. From the figure it is apparent that the Hoffman curve gives an acceptable representation for the advancing contact angle. Substituting this form into eq. (5) and solving for θ_2 gives

$$\cos\theta_2 = \cos\left(4.54Ca^{0.353}\right) - \frac{4l}{r}Ca \tag{14}$$

which shows θ_2 increasing with increasing Ca as is indicated in fig. 17. A similar expression could be obtained regardless of the static advancing and receding contact angles so long as an analytic form is available for θ_1. Since θ_2 cannot increase past the static receding value, an upper bound on Ca may be established for such capillary driven flows when $4l/r$ is known. As an example, the smallest value for $4l/r$ of this study was 22.5. For a static receding angle of 50°, eq. (14) when solved for Ca gives the peak value $Ca = 0.0024$, beyond which no flow could reach. This limit is indicated in fig. 15c as is eq. (14) for the maximum and minimum values of $4l/r$ used in these tests. The data are reasonably well bounded between the predicted limits and the value for $Ca \leq 0.0024$ is indeed the limit for the data set (refer also to fig. 14).

The increase of θ_2 with Ca is a result of the coupling between V and $\Delta\cos\theta$. Since Ca is determined naturally by the system it is not directly controlled as is often

the case for studies which drive the contact line and thereby force large values of Ca beyond that which the flow could attain naturally by capillarity alone. The fact that for these flows $Ca \propto \Delta \cos\theta$, it is no surprise that Ca is maximized for $\theta_2 \rightarrow \theta_{2_{stat}}$.

$\Delta \cos\theta$ can be scaled by its maximum value $\Delta \cos\theta_{ref} \equiv 1 - \cos\theta_{rec}$, where here θ_{rec} is the static receding contact angle and the advancing static angle has been set to 0. The contact angle values listed in table 2 are used to further reduce the data of fig. 16b and are replotted in fig. 18. For the fluid/solid/coating combinations selected for this study $\Delta \cos\theta / \Delta \cos\theta_{ref}$ centered around 0.51 with a standard deviation of 35% for all of the tests performed. This may provide an order of magnitude predictive capability to estimate V for a given test configuration, given that information concerning the static contact angles on the test surfaces is known.

Concluding Remarks

The cursory experimental results presented herein thoroughly demonstrate the steady nature of flows generated by discontinuously wetted tubes. This is most clearly seen from the individual tests performed (as an example, refer to fig. 6). The general agreement of eq. (11) with the complete data set in fig. 11 is also indicative of the accuracy of the simplified analysis over a wide parametric range, the scatter of the data about the predicted curve being due primarily to a large uncertainty $\sim \pm 25\%$ in the measurement of $\Delta \cos\theta$. Provided empirical data or analytic expressions are available for the advancing and receding contact angles as functions of Ca, eq. (4) may be solved directly for V. What is interesting here is the degree to which these flows are sensitive to tube surface conditions. For example, fig. 17 displays a three-fold increase in Ca for the PD condition. These results indicate the role of microscopic effects in the near vicinity of the contact line, since all else, including the static advancing and receding contact angles, is held constant. The technique of using surface coatings to produce steady capillary driven flows may serve well as a tool to probe the innerscale mechanisms controlling dynamic wetting.

The advantage of experimentation in the low gravity environment is that 'capillary' tubes can be quite large. Analytic models of such effects as surface roughness, surface cleanliness, patchy wettability, etc. on capillary driven flows could be further developed utilizing this test configuration since the internal conditions of the tubes can be quantified in detail. Tubes could be selected large enough that controlled surface roughness could be accurately machined, micro-fabricated through chemical deposition, selectively etched, etc. Thus, the low gravity environment presents further possibilities which, if exploited, could further our understanding of the complicated nature of capillary driven flows on non-idealized surfaces.

Acknowledgment

The author would like to especially thank J. Kadlowec, through Baldwin Wallace College, and A. White, a participant in the Summer High School Apprenticeship Research Program (SHARP) for their assistance in collection of the data. Discussions with R. Balasubramaniam are always appreciated.

References

1. *Satterlee, H.M., Reynolds, W.C.:* The Dynamics of the Free Liquid Surface in Cylindrical Containers under Strong Capillary and Weak Gravity Conditions, Dept. M.E. Stanford U., Tech. Report LG-2, Stanford, CA (1964)

2. *Kistler, S.F.:* in: Wettability, Surfactant Science Series, Vol. 49, J.C. Berg (Ed), Marcel Dekker, Inc., New York, p. 311/430 (1993) (see p. 348, p. 322 for Hoffman curve)

3. *Schwartz, L.W., Garoff, S.:* Contact Angle Hysteresis on Heterogeneous Surfaces, Langmuir, Vol. 1, No. 2, p. 219/230 (1985)

4. *Paterson, A., Fermigier, M., Jenffer, P., Limat, L.:* Wetting on heterogeneous surfaces: experiments in an imperfect Hele-Shaw cell, Physical Review E, Vol. 51, no. 2 pp 1291-8, Feb. 1995

5. *Hoffman, R.L.:* J. Col. Inter. Sci., 50:228 (1975)

6. *Washburn, E.W.:* The Dynamics of Capillary Flow, The Physical Review, 2nd Series XVII, Vol. 3, p. 273/283 (1921)

7. *Chaudhury, M., Whitesides, G.M.:* How to Make Water Run Uphill, Science, Vol. 256, p. 1539/1541, June 12 (1992)

8. *Mumley, T.E., Radke, C.J., Williams, M.C.:* Kinetics of Liquid/Liquid Capillary Rise, J. of Colloid and Int. Science, Parts I and II, Vol. 109, No. 2, p. 398/425, Feb. (1986)

9. *Weislogel, M.M., Ross H.D.:* Surface Reorientation and Settling in Cylinders upon Step Reduction in Gravity, Microgravity Sci. Technol. III, 1, p. 24/32 (1990)

Table 1. Tube data.

Tube Type	ID (±2%) (mm)	L (±2%) (mm)	$D_u \pm X$ (mm)	range of l tested (mm)
Straight (thin-walled)	0.516	95.0	–	6-79
	0.730	95.0	–	5-79
	1.145	95.0	–	39-42
	2.312	95.0	–	19-44
Straight (thick-walled)	1.08	212-481	–	60-303
	1.29	102	–	15-20
U-tubes	2.29	94, 121, 173, 206	10.3 (0.5)	61-101
	3.81	106, 133, 186	17.2 (1.0)	66-114
	5.94	113, 192, 140	22.0 (0.9)	79-121
	7.77	121, 139, 190, 206	22.6 (0.9)	85-133
	9.88	158, 206	32.2 (1.2)	119-134

Table 2. Properties of silicone oil test fluid on FC-723 coated glass.

$\nu \pm 2\%$ ($\times 10^{-6} m^2/s$)	$\rho \pm 5$ kg/m^3)	$\sigma \pm 5\%$ (N/m)	$\theta_{adv} \pm X$ ($deg.$)	$\theta_{rec} \pm X$ ($deg.$)
0.65	760	0.0159	44.7 (5)	35.0 (5)
1.0	816	0.0174	40.9 (2)	31.0 (2)
1.5	851	0.0180	51.7 (2)	41.7 (2)
2.0	872	0.0187	52.2 (2)	47.3 (2)
5.0	913	0.0197	57.4 (2)	48.9 (1)
10.0	935	0.0201	59.3 (3)	51.3 (2)
20.0	949	0.0206	56.0 (3)	46.2 (2)
50.0	960	0.0208	59.3 (3)	54.5 (2)
100.0	964	0.0209	–	–

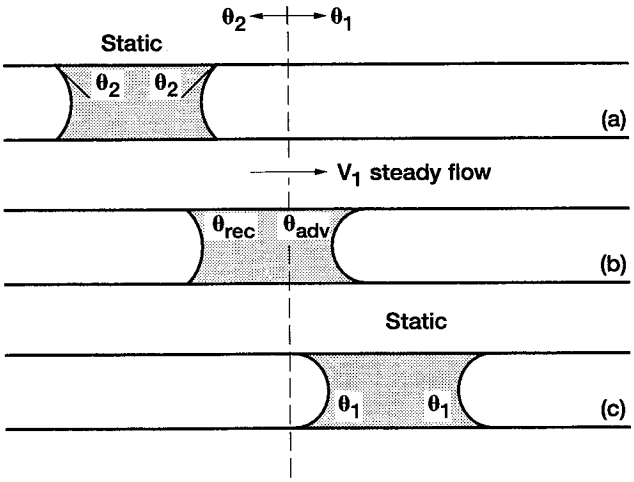

Figure 1.—Schematic of steady flow resulting from a dicontinuous wetting condition on the interior of a circular tube of constant radius where $\theta_1 < \theta_2$.

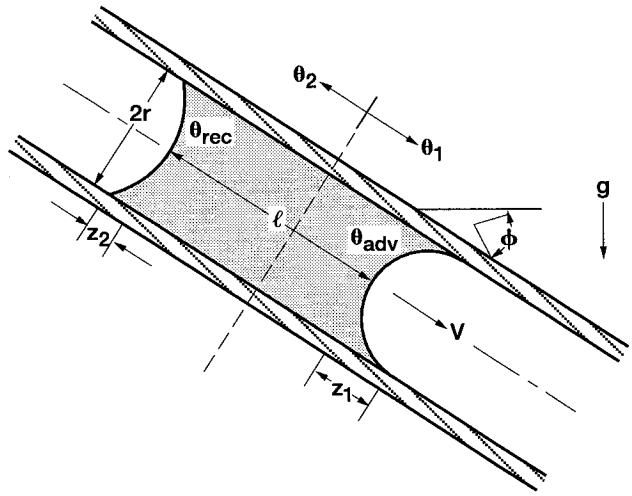

Figure 2.—Schematic of liquid slug of length l in a straight capillary tube of length L.

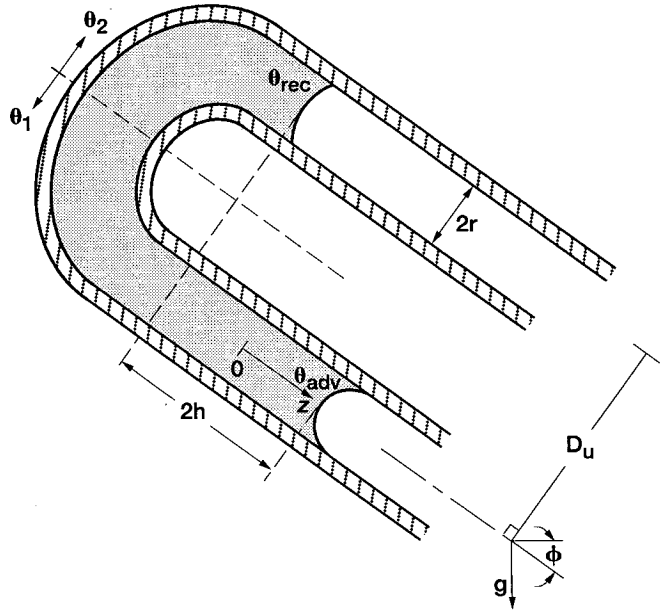

Figure 3.—Schematic of liquid slug in a U-tube where each leg of the 'U' has a different wettability with the fluid.

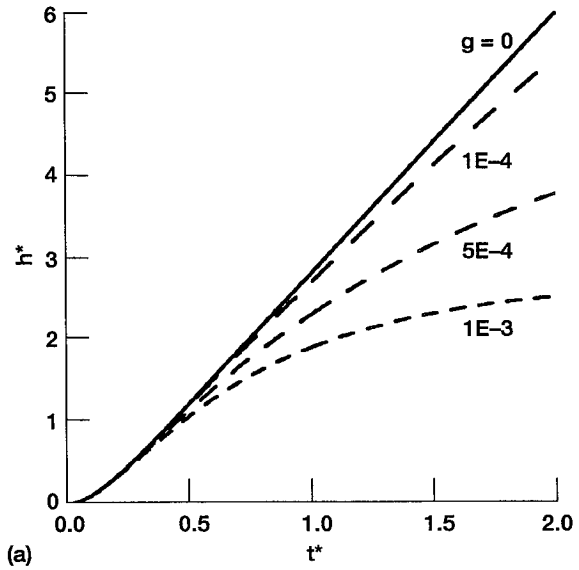

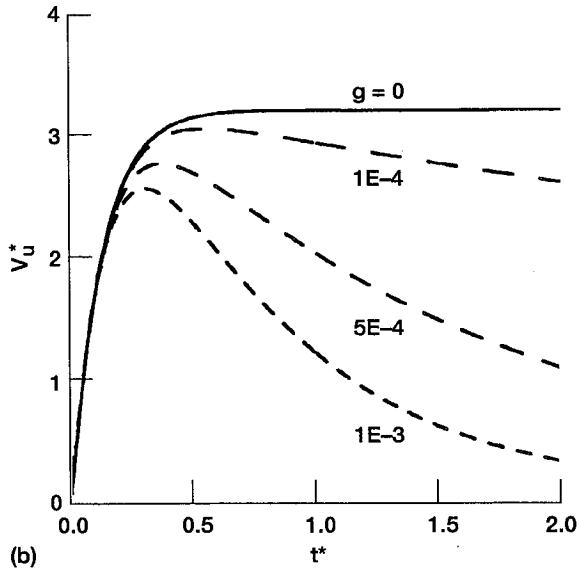

Figure 4a.—h*, and 4b. V_U^*, versus t*, respectively, for the U-tube configuration: effect of finite acceleration field, g (m/s^2).

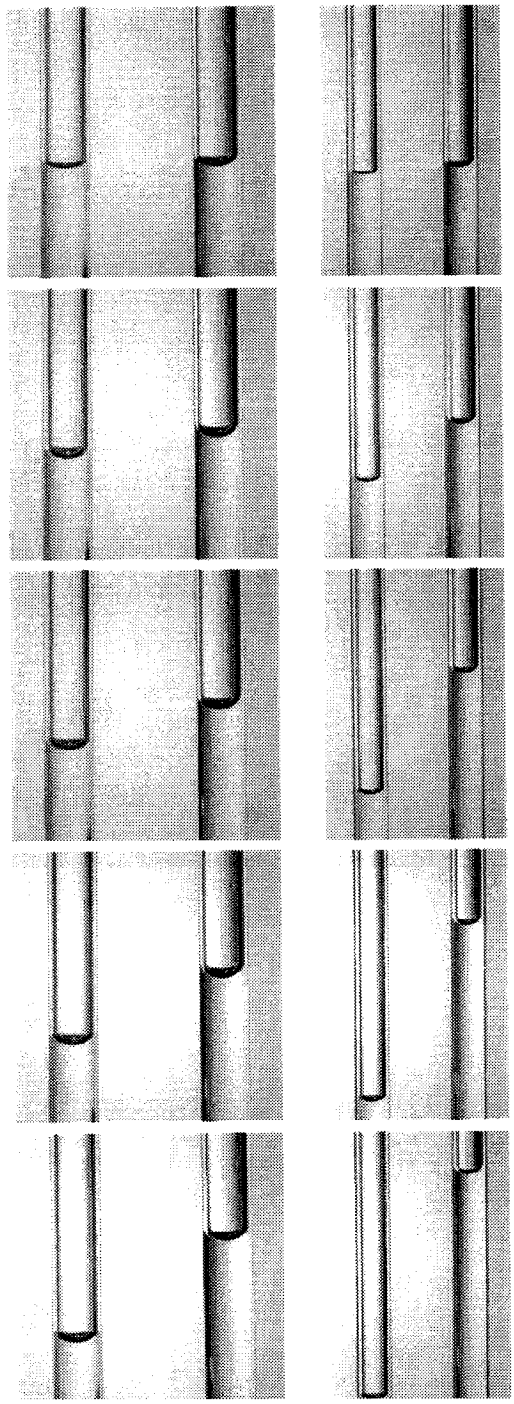

Figure 5.—Selected frames from two U-tube drop tower tests, ν = 1cS. Time progression is top to bottom in 0.5s increments, U-portion of tubes not pictured, and left legs of U-tubes are coated. [Left: r = 2.97, l = 121, L = 192 mm, V_u = 8.1 mm/s. Right: r = 1.90, l = 115, L = 186 mm, V_u = 3.2 mm/s.]

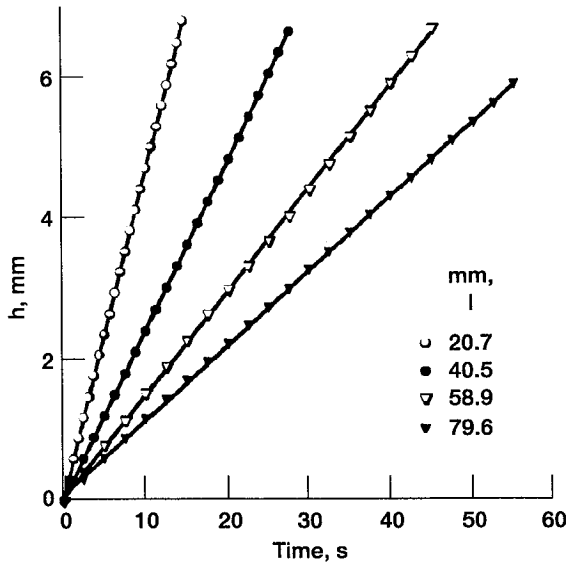

Figure 6.—h versus time for a variety of l's for ν = 1.0cS in a straight capillary tube, ID = 0.516 mm, factory cleaned condition. (Symbols are data, lines are linear fits.)

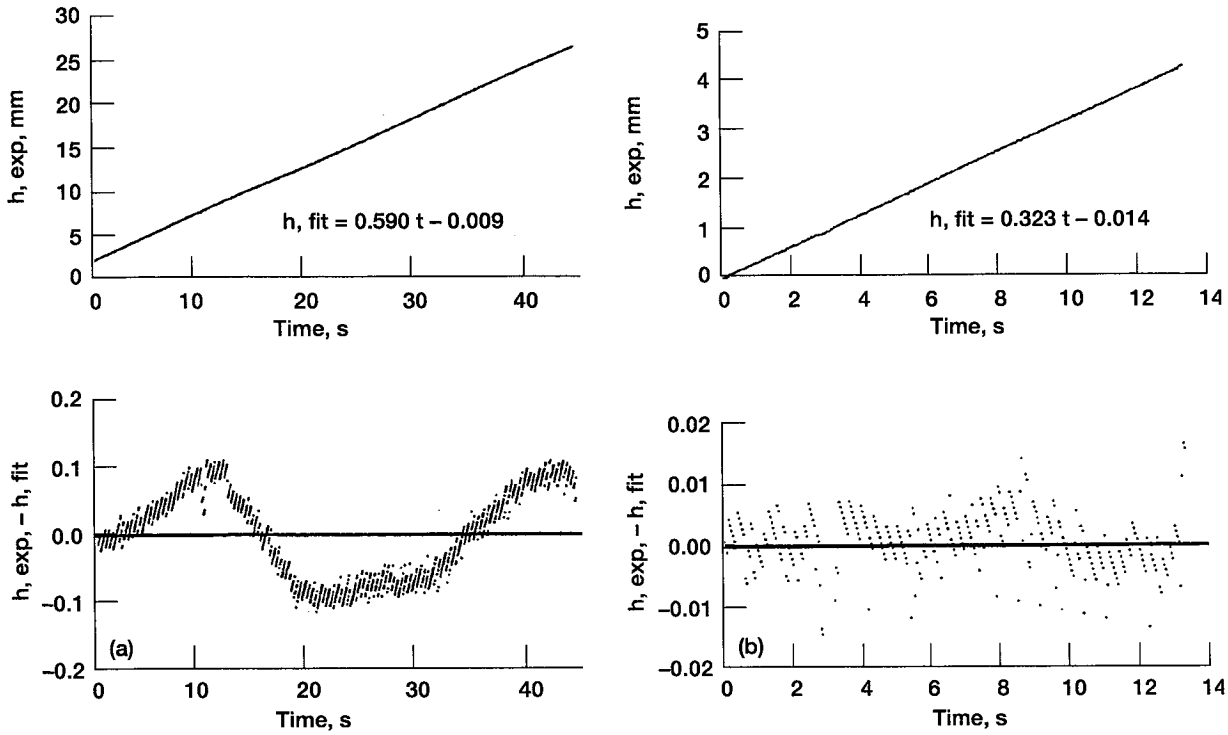

Figure 7.—Sample devitation plots of h (fit) with h (exp) for (D) factory cleaned straight tubes of ID = 1.08 mm. (a) ν = 0.65cS. (b) ν = 5cS.

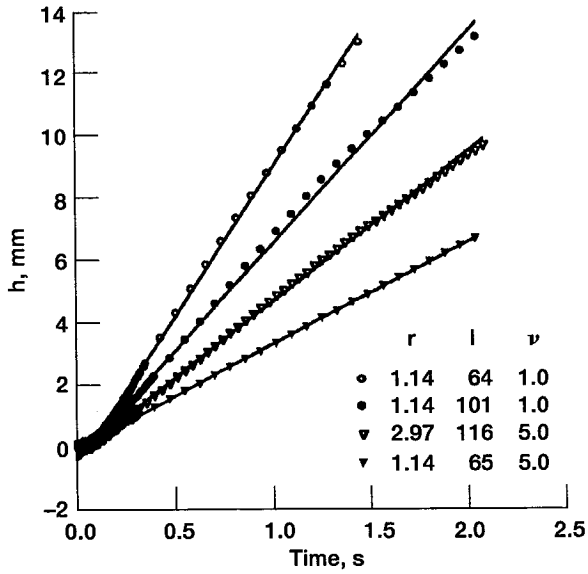

Figure 8.—Meniscus axial location versus time for several U-tube tests. (Lines are linear fits to the data above 0.25s.)

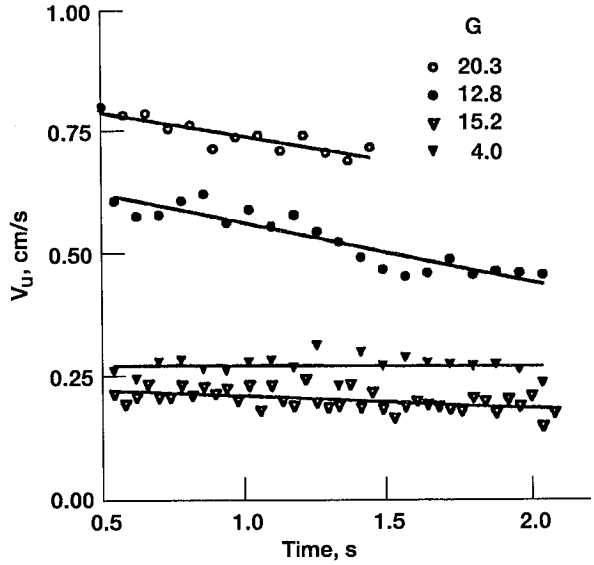

Figure 9.—Instantaneous velocity of liquid slug versus time for U-tube tests of fig. 8. Symbols are consistant with test conditions.

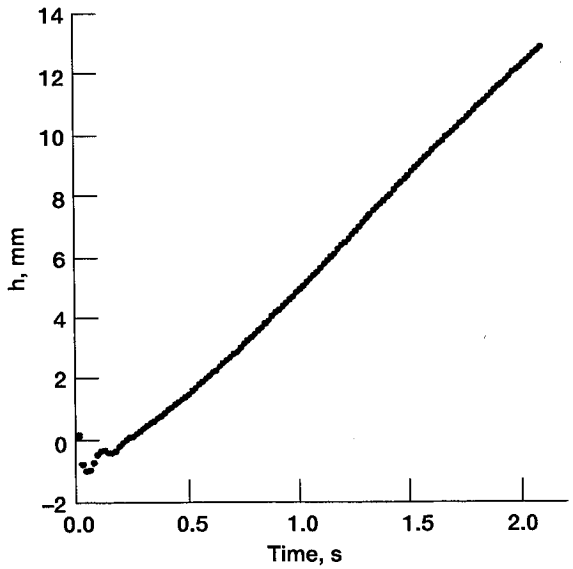

Figure 10.—Meniscus location for U-tube test of large radius, ν = 1cS, and r = 4.94, l = 131, and L = 206 mm.

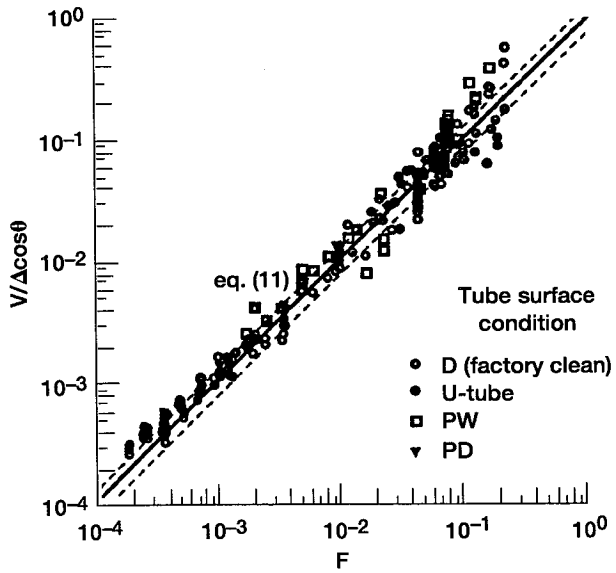

Figure 11.—V/Δcosθ versus F for tests performed.

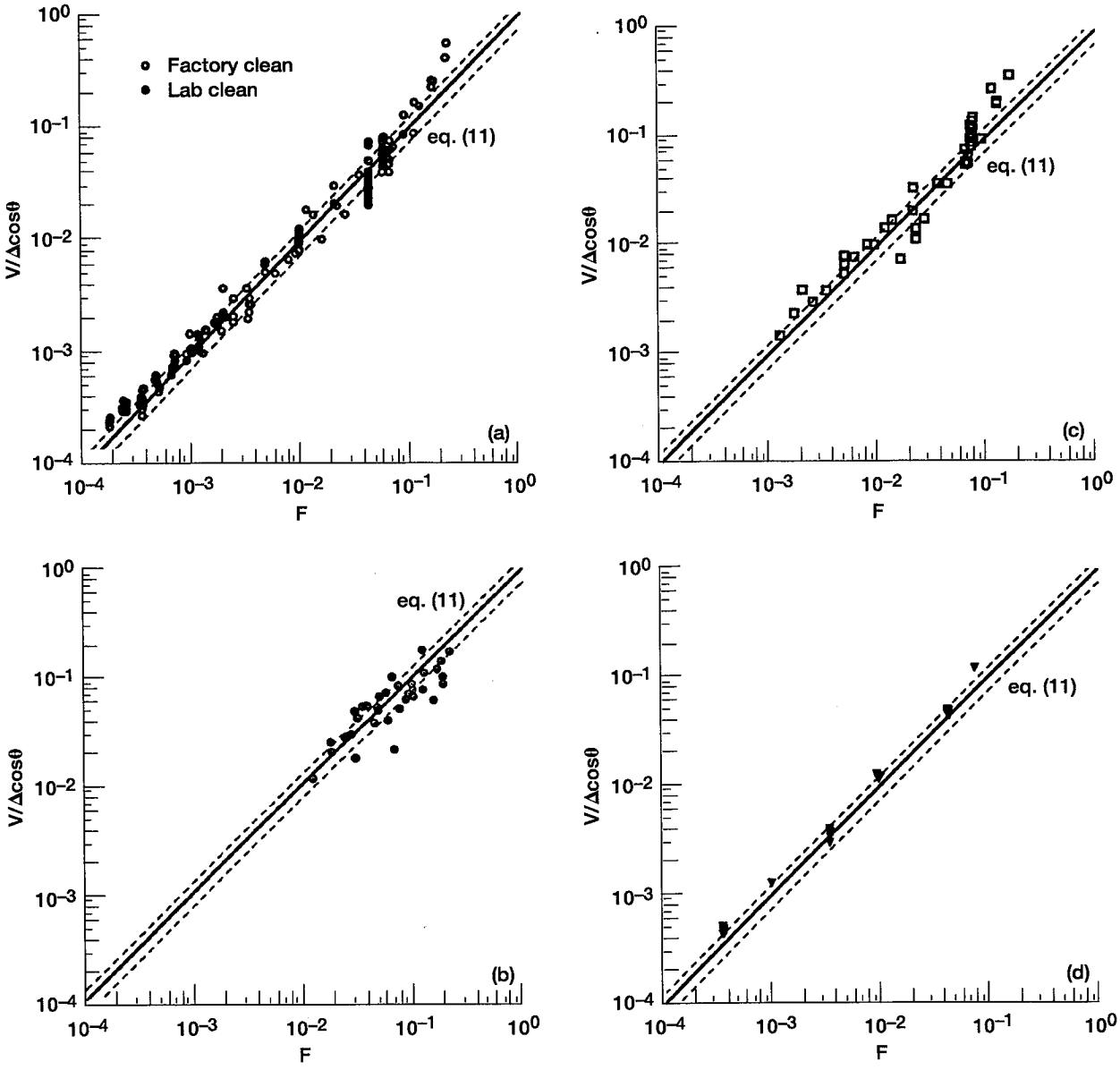

Figure 12.—Effect of tube tests and surface conditions for (a) D straight tubes, (b) U-tube tests, (c) PW straight tubes, and (d) PD straight tube tests.

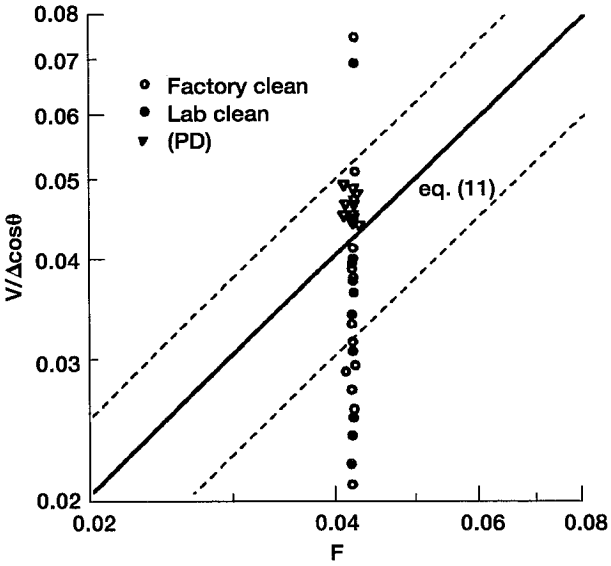

Figure 13.—Effect of tube cleaning condition for initially 'dry' tubes.

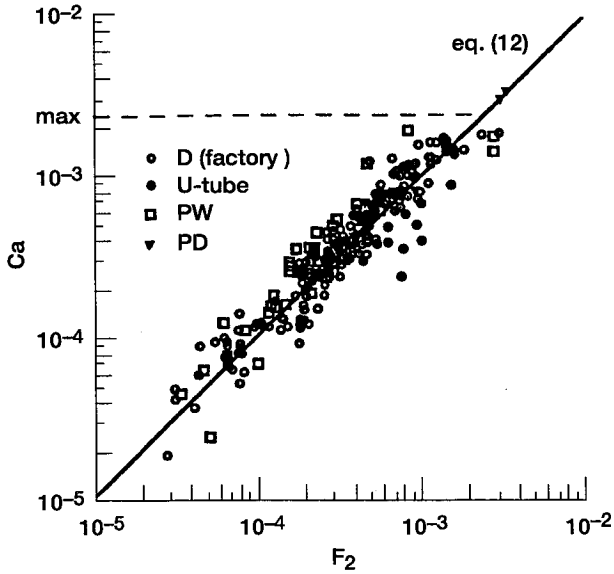

Figure 14.—Capillary number as a function of F_2.

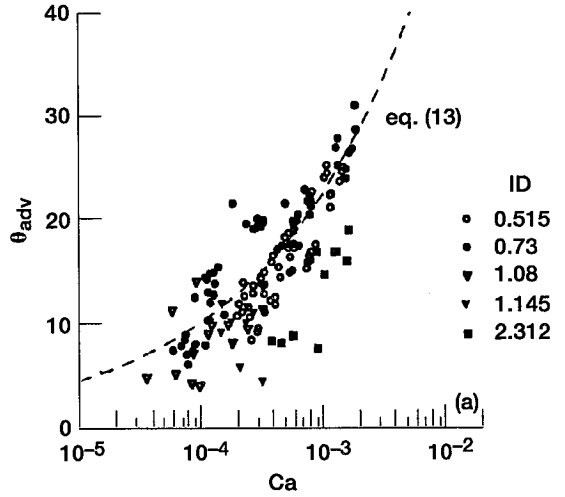

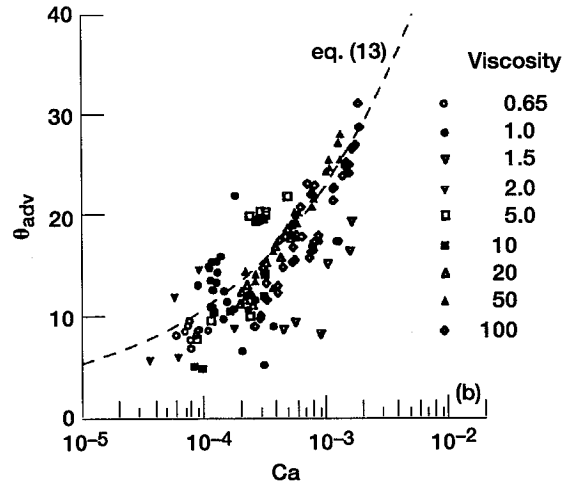

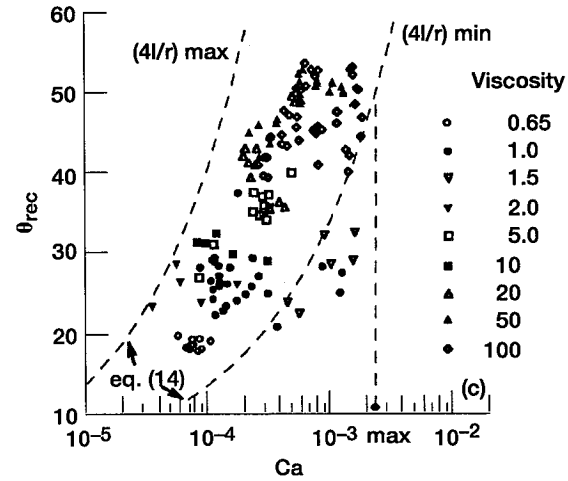

Figure 15.—Ca dependence of (a) θ_{adv} ID indicated, (b) θ_{adv} viscosity indicated, and (c) θ_{rec} viscosity indicated for factory cleaned (D) straight tubes.

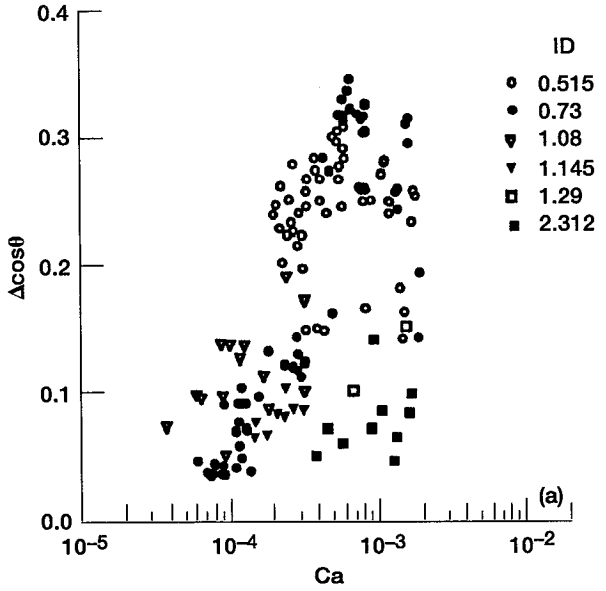

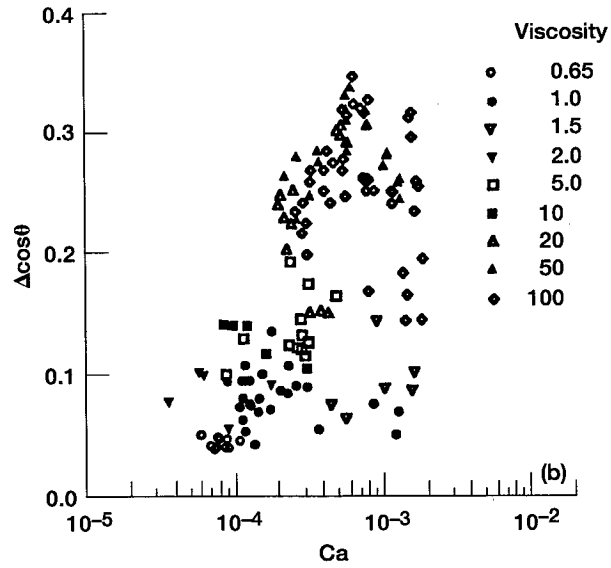

Figure 16.—Δcosθ versus Ca for factory cleaned (D) straight tubes, (a) ID indicated, (b) viscosity indicated.

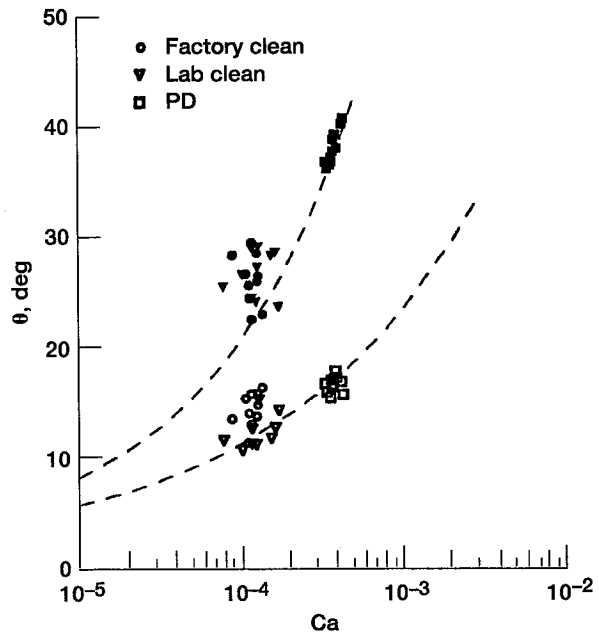

Figure 17.—Dynamic contact angle versus Ca for fixed F, data of fig. 13. Hollow symbols are advancing values, solids are receding. (4l/r = 438.)

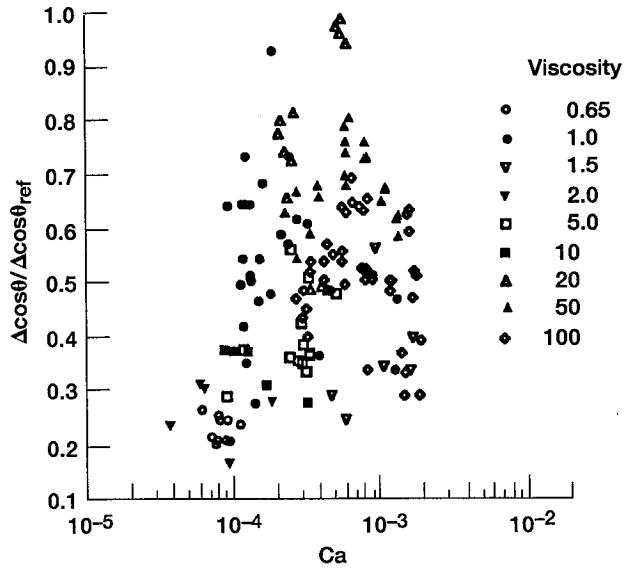

Figure 18.—Reduced Δcosθ versus Ca for data of fig. 16b.

REPORT DOCUMENTATION PAGE

Form Approved
OMB No. 0704-0188

1. AGENCY USE ONLY (*Leave blank*)	2. REPORT DATE	3. REPORT TYPE AND DATES COVERED
	February 1996	Technical Memorandum

4. TITLE AND SUBTITLE

Steady Capillary Driven Flow

5. FUNDING NUMBERS

WU–962–24–00

6. AUTHOR(S)

Mark M. Weislogel

7. PERFORMING ORGANIZATION NAME(S) AND ADDRESS(ES)

National Aeronautics and Space Administration
Lewis Research Center
Cleveland, Ohio 44135–3191

8. PERFORMING ORGANIZATION REPORT NUMBER

E–10078

9. SPONSORING/MONITORING AGENCY NAME(S) AND ADDRESS(ES)

National Aeronautics and Space Administration
Washington, D.C. 20546–0001

10. SPONSORING/MONITORING AGENCY REPORT NUMBER

NASA TM–107146

11. SUPPLEMENTARY NOTES

Responsible person, Mark M. Weislogel, organization code 6712, (216) 433–2877.

12a. DISTRIBUTION/AVAILABILITY STATEMENT

Unclassified - Unlimited
Subject Categories 34 and 28

This publication is available from the NASA Center for Aerospace Information, (301) 621–0390.

12b. DISTRIBUTION CODE

13. ABSTRACT ***(Maximum 200 words)***

A steady capillary driven flow is developed for a liquid index in a circular tube which is partially coated with a surface modifier to produce a discontinuous wetting condition from one side of the tube to the other. The bulk flow is novel in that it is truly steady, and controlled solely by the physics associated with dynamic wetting. The influence of gravity on the flow is minimized through the use of small diameter tubes $\sim O(1mm)$ tested horizontally in a laboratory and larger tubes $\sim O(10mm)$ tested in the low gravity environment of a drop tower. Average steady velocities are predicted and compared against a large experimental data set which includes the effects of tube dimensions and fluid properties. The sensitivity of the velocity to surface cleanliness is dramatic and the advantages of experimentation in a microgravity environment are discussed.

14. SUBJECT TERMS

Reduced gravity drop towers; Interfacial tension; Wetting; Steady flow; Coatings; Capillary flow; Tubes

15. NUMBER OF PAGES

23

16. PRICE CODE

A03

17. SECURITY CLASSIFICATION OF REPORT	18. SECURITY CLASSIFICATION OF THIS PAGE	19. SECURITY CLASSIFICATION OF ABSTRACT	20. LIMITATION OF ABSTRACT
Unclassified	Unclassified	Unclassified	